17

Buoyant Outflows to the Coastal Ocean*

Pablo Huq
University of Delaware

17.1 Introduction

Buoyant freshwater outflows from rivers, estuaries, or straits that results in extended offshore areas of low salinity waters. The influence of the low salinity strongly impacts the ecology of coastal waters, thereby affecting fisheries and the economies dependent on them. These buoyant outflows can form large recirculating bulges and downshelf propagating coastal currents. Here we review the progress in understanding the dynamics of bulges and coastal currents arising from buoyant outflows to the coastal ocean.

Typically, the waters of such freshwater outflows contain chemicals such as nitrates and phosphorous from agricultural runoff. Such chemicals adversely impact the health of the coastal ecosystem. Excessive amounts of nitrates and phosphorous can lead to the depletion of oxygen in coastal waters coupled to such outflows. The resulting anoxia and hypoxia of coastal waters is a worldwide problem. Thus, knowledge of transport rates and details of the structure of the freshwater flow through the coastal ocean is an important component of the dynamics as well as in the evaluation of fluxes of chemicals, biological materials, and sediments from land to the deep ocean.

Buoyant outflow to the coastal ocean is a multifaceted problem. Flows are driven principally by wind stress, density differences between the buoyant outflow and the ambient coastal ocean, and heat fluxes at the sea-surface. The Earth's rotation (i.e., Coriolis force), tides, and turbulent mixing further complicate the dynamics. These forcings were discussed in "The Sea Volume 10—Global Coastal Ocean," edited by Brink and Robinson (1998). The focus of this review of buoyant outflows to the coastal ocean is to discuss the role of the geometry of the outflow—in particular, the effects of the bottom slope, α, of the continental shelf; the angle, θ, of the longitudinal axis of the buoyant outflow to the downshelf coast; and the radius of curvature, r_c, of the coastline at the exit of the outflow. The interplay between these geometric variables influences the transport and path of the buoyant outflow.

The transport of suspended biota and sediments from the estuary to the coastal ocean depends on the "flow pathways" in the vicinity of the outflow exit. For example, observations have established that one flow pathway is the buoyancy-driven coastal current that can often form downshelf of the exit. (Downshelf is defined as the direction of Kelvin wave propagation. Downshelf is to the right in the northern hemisphere and to the left in the southern hemisphere.) Mean hydrographic properties of these coastal currents have been established from observations of the Alaskan coastal current, the Chesapeake Bay outflow, the Columbia River plume, the Connecticut River outflow, the Delaware coastal current, the Gaspe coastal current, the Hudson River outflow, the Rhine outflow, the Rio de la Plata outflow, the Scottish coastal current, the South Atlantic Bight river outflows, and the Vancouver Island coastal current. Figure 17.1 shows the coastal current that forms as the buoyant warm water flows through the Tsugaru Strait between Hokkaido and Honshu islands in Japan. It exits at Cape Shiriya and turns and flows southwards down the Sanriku coast in north-east Honshu.

Figure 17.1 also shows a second feature, a flow pathway that sometimes exists at the exit of buoyant outflows in the form

* *Handbook of Environmental Fluid Dynamics, Volume One*, edited by H. J. S. Fernando. © 2013 CRC Press/Taylor & Francis Group, LLC. ISBN: 978-1-4398-1669-1.

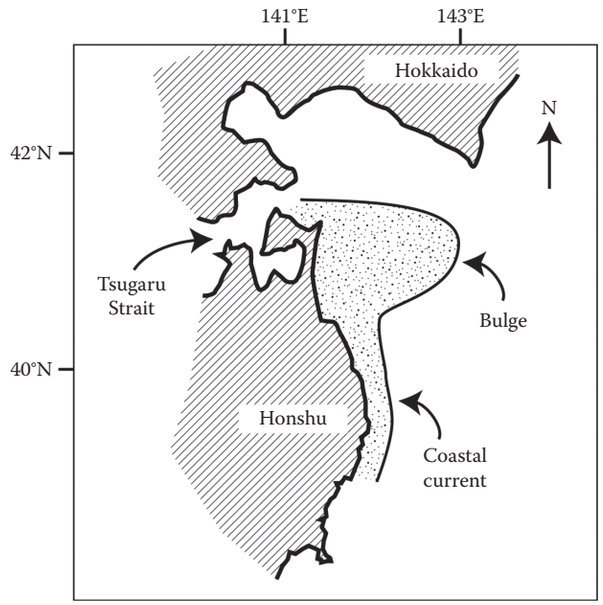

FIGURE 17.1 This shows the buoyant outflow exiting from the Tsugaru Strait in Japan in summer and autumn. Evident are a bulge and a coastal current further downshelf. (Adapted from Sugimoto, T., A review of recent physical investigation of straits around the Japanese Islands, in *The Physical Oceanography of Sea Straits*, ed., Pratt, L.J., Kluwer Academic, Dordrecht, the Netherlands, 1990.)

of a recirculating gyre or bulge. Details of this bulge feature are shown in Figure 17.2 of the contours of isotherms (°C) at a depth of 200 m of the bulge that forms during summer and autumn offshore of Cape Shiriya at the exit of Tsugaru Strait. The distribution of isotherms of the bulge is circular,

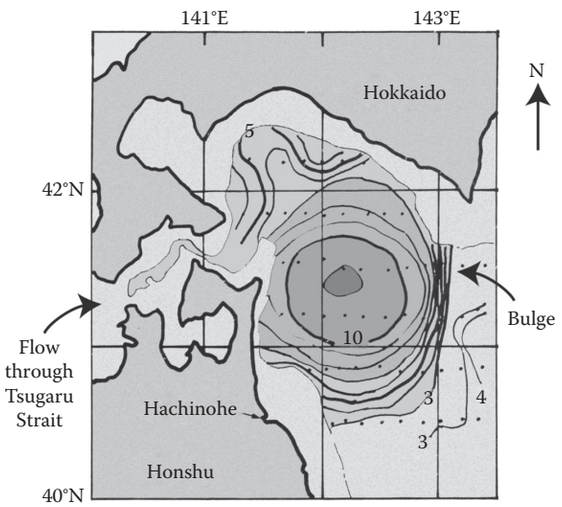

FIGURE 17.2 Detailed hydrography of the Tsugaru Bulge located offshore of Cape Shiriya. Shown are contours of temperature (°C) at 200 m. (Adapted from *Ocean Hydrodynamics of the Japan and East China Seas*, Kawasaki, Y. and Sugimoto, T., Experimental studies on the formation and degeneration process of the Tsugaru Warm Gyre, pp. 225–238, Copyright 1984, Elsevier.)

and of large scale—150 km in diameter and at least 200 m in depth. A consequence is that a large fraction of the buoyant water flowing through Tsugaru Strait is stored in the bulge. In the results discussed later in this review, it is demonstrated that such storage attenuates the scales of the coastal current. Bulges are characterized by anticyclonic vorticity, and their dynamics involve a cyclostrophic balance (Yankovsky and Chapman 1997).

It has been established that the geometry of the coastline, in particular the radius of curvature of the coastline and the outflow angle to the coastline, influences whether or not bulges form (Avicola and Huq 2003a,b; Horner-Devine et al. 2006). A schematic of a buoyant outflow to the coastal ocean is shown in Figure 17.3 to introduce the notation of this review. This shows a buoyant outflow (of typical density $(\rho_o - \Delta\rho)$ that exits from a river, estuary, or strait to a coastal ocean of typical density ρ_o. Thus the density anomaly is $\Delta\rho$. The offshore direction is y, and the downshelf direction is x, and the Coriolis parameter is f. The angle θ is the angle between the longitudinal axis of the buoyant outflow and the downshelf coastline. The local radius of curvature at the exit on the downshelf side is r_c. A region of extended offshore extent of buoyant water is designated as the bulge. Downshelf of the bulge is a propagating coastal current of offshore width γL and alongshore length L (the value of the slenderness ratio γ is less than one).

Hydrodynamic equations governing buoyant outflows are introduced in Section 17.2. A brief description of the rotating tank apparatus used for the laboratory experiments to simulate buoyant outflows follows in Section 17.3. Two sets of results are presented in Section 17.4. Discussed first are criterion for when bulges form and bulge characteristics. The scaling analysis of downshelf propagating coastal currents, and oceanic observations are considered in the second half of Section 17.4. Outstanding issues and challenges for the future are summarized in the concluding Section 17.5.

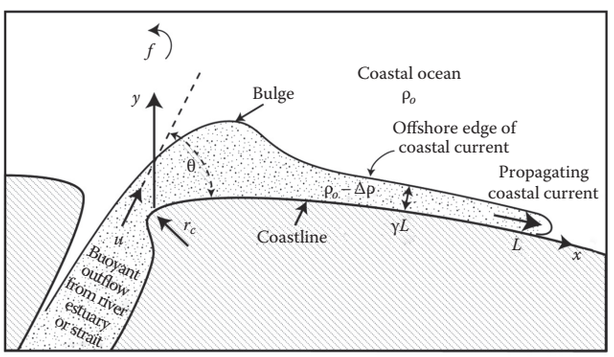

FIGURE 17.3 Schematic of bulge and coastal current arising from buoyant outflow from a river, estuary, or ocean. Buoyant outflow of density $(\rho_o - \Delta\rho)$ exits at a velocity u to a coastal ocean of density ρ_o. x and y are the alongshore and offshore coordinates. The axis of the buoyant outflow is at an angle θ to the downshelf coastline. At the exit, the radius of curvature to the local coastline is r_c. The width γL of the coastal current is smaller than its length L. The Coriolis parameter is f.

17.2 Principles

Buoyant outflows to the coastal ocean are deflected by the influence of Earth's rotation and flow downshelf along a coastline in the direction of Kelvin wave propagation. The dynamics involves rotation, pressure gradients, and friction. Forcing can also include winds and tides. The conventional approach is to consider two layers of differing densities—($\rho_o - \Delta\rho$) for the buoyant layer of depth h, and ρ_o for the coastal ocean of depth H. For simplicity, a steady-state analysis with a constant outflow Q is undertaken. Tides and variability of winds are neglected. Garvine (1995) utilized a framework of continuity and vertically integrated continuity equations to describe the flow.

$$\frac{\partial}{\partial x}(hu) + \frac{\partial}{\partial y}(hv) = 0 \tag{17.1}$$

This neglects entrainment or mixing into the buoyant layer h. Oceanic observations of buoyant outflows show a slender flow whose offshore width of the buoyant layer is smaller than its downshelf length (i.e., transverse velocity v is smaller than longitudinal velocity u). So

$$v \sim \gamma u \tag{17.2}$$

Vertically averaged equations in the longitudinal (x) and offshore (y) directions are

$$\frac{\partial}{\partial x}(u^2) + \frac{\partial}{\partial y}(uv) - fv = -\frac{1}{\rho_o}\frac{\partial p}{\partial x} + \frac{\tau_w^{(x)}}{\rho_o h} - \frac{\tau_b^{(x)}}{\rho_o h} \tag{17.3a}$$

$$\frac{\partial}{\partial x}(uv) + \frac{\partial}{\partial y}(v^2) + fu = -\frac{1}{\rho_o}\frac{\partial p}{\partial y} + \frac{\tau_w^{(y)}}{\rho_o h} - \frac{\tau_b^{(y)}}{\rho_o h} \tag{17.3b}$$

where

f is the Coriolis parameter
p is the pressure
τ_w and τ_b are wind and bottom stress decomposed into the x and y direction

Scaling yields dimensionless numbers characterizing the flow. $\gamma \sim v/u$ is the slenderness ratio of the offshore to downshelf velocities. The Kelvin number $K = (\gamma L/R)$ is the ratio of the across-shelf length scale to the internal Rossby radius R. (Here $R = c/f$ with internal wave speed $c = (g'h)^{1/2}$ where h is the depth of the buoyant layer and g' is the reduced gravitational acceleration.) The internal Rossby radius R is the horizontal scale at which the effects of rotation become as important as restoring buoyancy. For outflows with $K > 1$ the dynamics are rotational, whereas for $K < 1$ the influence of the Coriolis force is small. The Rossby number $R_o = u/f\gamma L$ reflects the relative balance of nonlinear advection to Coriolis force. For $R_o \ll 1$, the dynamics of the flow field are linear. The Froude number $F = u/c$ is a measure of the importance of inertial and buoyancy forces. The value of the ratio (h/H) of the buoyant layer depth to the total oceanic depth establishes the buoyant outflows as either surface-advected ($h/H \sim 0.1$) or bottom-advected buoyant outflows ($h/H \sim 1.0$).

To summarize, the parameters describing the dynamics of rotating buoyant outflows include h/H, K, R_o, F. Wind and bottom stress may form Ekman layers at the top and bottom of the ocean. Thus friction contributes near boundaries; this is parameterized by the Ekman number $E_k \sim A_v/(fH^2)$, where A_v is a turbulent eddy viscosity. The different forcings and the large number of the parameters allow for the likelihood of future discovery of new flow phenomena. Presently known phenomena include flow separation, formation of bulges, and/or coastal currents.

17.3 Methods of Analysis

Numerical models such as ROMS (Regional Ocean Model System) are a popular analysis tool. They are based on the governing hydrodynamic equations. With regard to buoyant outflows exiting to the coastal ocean, there are little observational data on lateral velocity and density profiles across the exit to guide the specification of model boundary conditions. Thus a laboratory rotating tank model is useful to examine the role of geometry and bathymetry on the dynamics of buoyant outflows. Changes in exit angle θ, and radius of curvature r_c and fractional depth h/H are readily implemented in such studies. To isolate the effects of coastline geometry, we focus on buoyant outflows under conditions of weak winds and tides. Such conditions are set up by placing a Plexiglas sheet over the top of the tank to prevent wind-stress-induced motions, and balancing the entire rotating tank facility to minimize tidal motions.

The apparatus for two sets of laboratory experiments are described briefly. The first set examines flow separation, bulge formation, and their characteristics; the second set describes the scaling of coastal currents. For the first set, laboratory experiments are conducted on a large, flat-bottomed, rotating cylindrical tank. To simulate a river, estuary, or strait to the coastal ocean, a box is welded to the perimeter of the tank (see Figure 17.4b). The walls of the box make a 90° angle with the wall of the tank. False walls are available for placement within the box, which allows experiments to be performed with varying exit angles, θ, outflow widths, W, and radius of curvature, r_c, at the exit of the outflow to the coastal ocean. Buoyant outflow of density ($\rho_o - \Delta\rho$) is introduced through a pipe at the most upstream end of the box at a known outflow rate Q from a freshwater reservoir that co-rotates with the rotating tank. The tank rotates at a specified rotation rate, f, which can be carefully controlled. The tank (i.e., the coastal ocean) is filled with salt water of density ρ_o to a depth H, and allowed to spin up to solid body rotation before experiments are conducted. The value of the fractional depth h/H of the buoyant layer to the total depth was 0.1, so that the buoyant outflows of the first set of experiments are surface-advected; the exit Kelvin number $K_e = W/R = 1$.

The second set of experiments was similar to the first, except the box is closed off—so that the tank's plan geometry is circular. The source, a pipe, discharged parallel to the wall (i.e., coast).

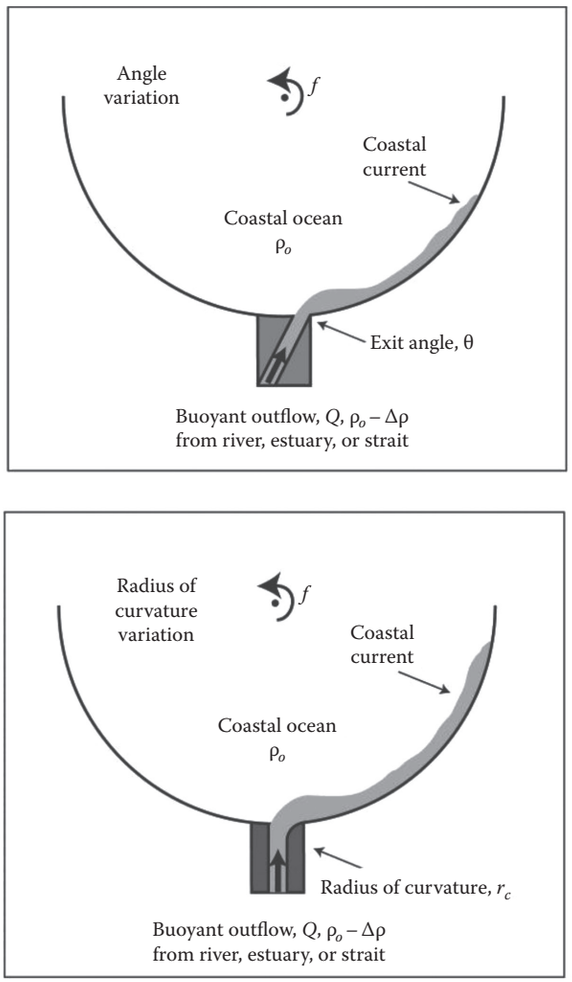

FIGURE 17.4 Schematics of rotating turntable experiment of buoyant outflows to the coastal ocean. The dark area is a box that is welded to the perimeter of a cylindrical tank. The panels (a) and (b) show buoyant outflow configurations with variation of exit angle θ or variation of radius of curvature. (Adapted from Avicola, G. and Huq, P., *J. Marine Res.*, 61, 435, 2003a.)

Experiments were conducted with a flat-bottomed tank and also a tank with a sloping-bottom for the second set of experiments so as to discriminate the effects of the slope (i.e., vortex stretching). The fractional depth h/H varied between about 0.1–1 spanning the range between surface- and bottom-advected outflows. (See Figure 17.11 for a schematic of the flow field of the second set of experiments.)

The rotating tank facility is equipped to interrogate buoyant outflows. Whole field velocity measurements are obtained through the Particle Image Velocimetry (PIV) technique utilizing surface drifters. A digital camera in conjunction with a PC is utilized to record visualizations and analyze the experiments. In addition, 3D density fields are determined from density transects using traversing micro-probes.

Vertical, horizontal, and velocity scales are nondimensionalized by the scale depth of the buoyant layer h, the internal Rossby radius R, and the internal wave speed c. Here,

$$h = \sqrt{\frac{2Qf}{g'}} \quad R = \frac{\sqrt{g'h}}{f} \quad c = \sqrt{g'h} \tag{17.4}$$

finally, time t is nondimensionalized by the rotation period of the rotating turntable $T = 4\pi/f$ so that $t/T = 1$ is equivalent to a day.

17.4 Applications/Results

A general configuration for buoyant outflow exiting to the coastal sea is shown in Figure 17.5. Results to follow can be used to make predictions for coastal buoyant outflows if scales such as the internal Rossby radius R and flow rate Q, etc., are known.

17.4.1 Flow Separation

The radius of curvature at the exit is r_c. The trajectory of the outflow is deflected by the Coriolis force: the exiting buoyant outflow follows an inertial circle of radius u/f. The ratio of the radius of curvature to the radius of the inertial circle is important in determining whether the buoyant outflow will separate from the coastline. If r_c is smaller than u/f, then the flow will separate from the right coastline. (In the southern hemisphere it will separate from the left coastline.) The ratio of radii forms the exit Rossby number $R_o = u/fr_c$; for values of R_o greater than one, flow separation occurs. The buoyant outflow impacts or reattaches to the coastline further downshelf from the exit at an angle φ.

The exit angle, θ, of the outflow to the coastline also influences flow separation. Buoyant outflows emerging perpendicular or at obtuse angles to the coastline are more likely to separate than flows exiting at acute angles to the coastline. Also the

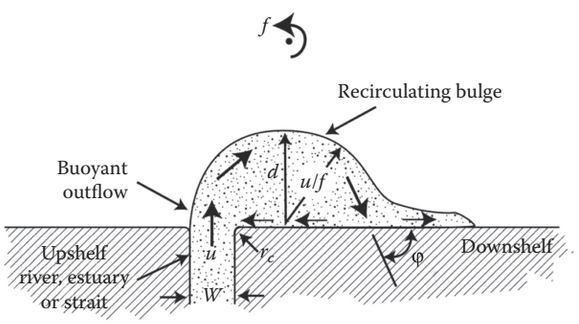

FIGURE 17.5 Schematic of a buoyant outflow from a river, estuary, or strait. The width of the exit is W; the velocity at the exit is u; the radius of curvature between the exit and the coastline is r_c. The buoyant outflow forms a recirculating, semicircular bulge of radius d. Also shown is an inertial circle of radius u/f. As drawn $d = u/f$. The buoyant outflow recirculates and impacts the downshelf coastline at an angle φ. A fraction of the buoyant outflow recirculates toward the source, with the remainder forming a coastal current which propagates downshelf.

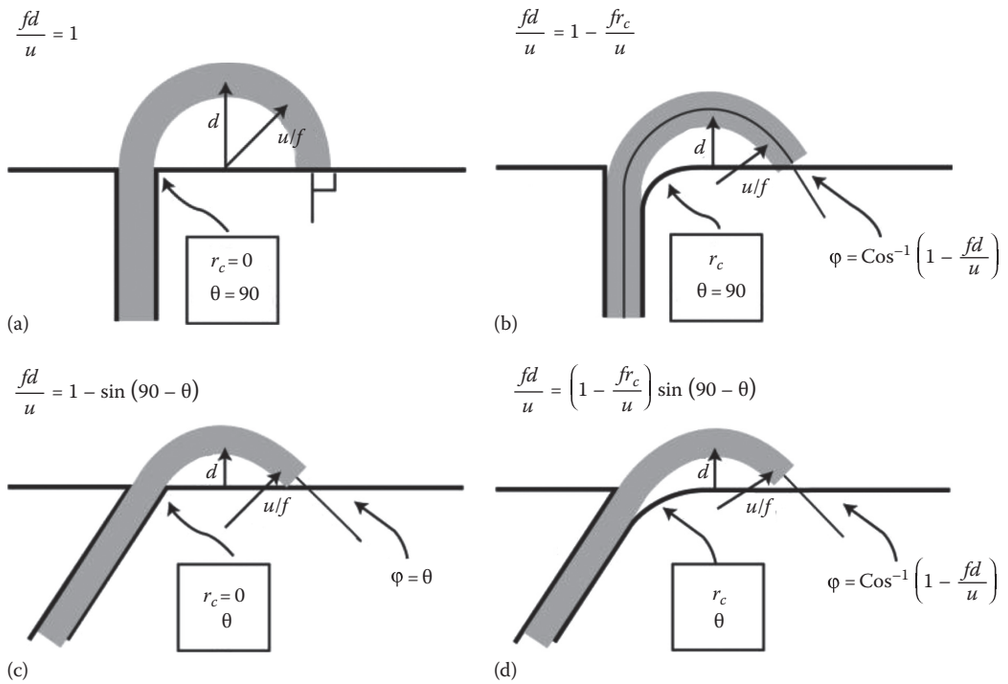

FIGURE 17.6 Schematics of the trajectory of the buoyant outflow (thick shaded line) are shown for various permutations of exit angle θ, radius of curvature r_c, and inertial circle *u/f*; these variables determine the downshelf impact angle φ. The upper panels depict an outflow exiting perpendicularly to the coastline (θ = 90°); the lower panels are for outflows exiting at angle (90 − θ) to the coastline. Panels (a) and (c) describe sharp-cornered exits with zero radius of curvature r_c; panels (b) and (d) have non-zero r_c. General expressions for the separation ratio *fd/u* and impact angle φ are also given. (Adapted from Avicola, G. and Huq, P., *J. Marine Res*., 61, 435, 2003a.)

offshore extent, *d*, of outflows perpendicular to the coastline is greater than outflows exiting parallel to the coastline. Different scenarios or configurations arising from combinations of *u/f*, r_c, and θ are shown in Figure 17.6.

Figure 17.6a and b show configurations with an exit angle θ = 90°, and cases with negligible and finite values of radius of curvature r_c. The lower panels show the situation for cases when θ ≠ 90° with negligible and finite values of r_c. The combined effects of the exit angle and radius of curvature can be examined in terms of the ratio Γ = *df/u*. The value of Γ varies between zero and one; buoyant outflows do not separate for Γ = 0. Maximum values of Γ occur when the separation distance *d* is equal to the inertial turn radius r_c. If buoyant outflows do not separate from the coastline, then only coastal currents are likely. Conversely, if flow separation occurs, then a flow with both a bulge and a coastal current are likely. Experimental data suggest a critical value of Γ = 0.5 (see Figure 17.7).

The shaded trajectory of the buoyant outflow in Figure 17.6 suggests that the flow approach to the downshelf coastline is perpendicular when the separation distance *d* is equal to the inertial radius *f/u* (Figure 17.6a). In contrast, the approach is less than perpendicular and more parallel to the coastline for separation distances less than the inertial radius. Thus, the separation ratio Γ can also be interpreted in terms of the impact angle $\varphi = \cos^{-1}(1 - fd/u)$ at which the buoyant outflow impacts the coastline. This is useful as the magnitude of φ determines

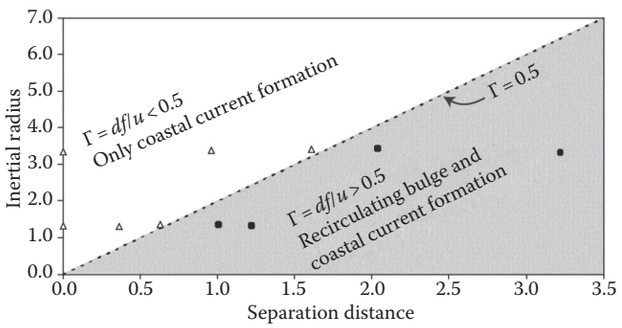

FIGURE 17.7 Comparison of predicted inertial radius *f/u* and separation distance *d*. The line Γ = 0.5 delineates flows where only coastal currents form from flows where both bulges and coastal currents form. Coastal currents only formed for Γ < 0.5 (triangles); both recirculating bulge and coastal currents form for Γ > 0.5 (circles in shaded region). (Adapted from Avicola, G. and Huq, P., *J. Marine Res*., 61, 435, 2003a.)

whether or not bulges form and so determines flow pathways. The dynamics of the point of impact has been analyzed as the deflection of a baroclinic jet by a wall in a rotating frame of reference (Whitehead 1985). Analysis showed that volume and momentum fluxes are increasingly recirculated back toward the outflow exit with increasing impact angle φ (see Figure 17.8). For φ > 60° more than 50% of the volume flux is recirculated: this promotes bulge formation. The balance or remaining volume

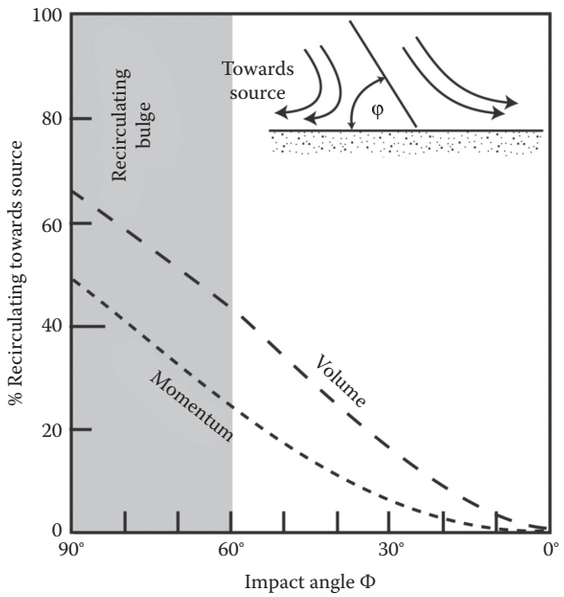

FIGURE 17.8 Schematic of fluxes for a buoyant flow impacting a wall. Shown is a plot of percentage of momentum and volume flux returning to the source region as a function of impact angle φ. Recirculating bulges form for impact angles greater than 60° as indicated by the shaded region.

flux propagates downshelf as a coastal current. The recirculation of the flow has obvious consequences. For example, the residence times of fluid in the bulge will be much longer than estimates based solely on advection.

17.4.2 Characteristics of Bulges

When bulges form, they are among the largest coherent structures in the coastal ocean. Figure 17.2 shows that the bulge forming at the exit of the Tsugaru Strait is approximately 150 km. They are crucially important to the dynamics and biology of the coastal ocean. Experimental data of the evolution of the bulge length, width, depth, and volume are presented in nondimensional form in Figure 17.9 so as to allow comparison with field data. Nondimensional length and width of the bulge evolved as $t^{0.40}$, and depth evolved as $t^{0.16}$. It is insightful to compare the dynamics of a recirculating bulge with that of a stable buoyant lens (or vortex) formed from a constant volume flux source. This yields growth rates of radius evolving as $t^{1/4}$ and depth evolving as $t^{1/2}$ (Nof and Pichevin 2001; Avicola and Huq 2003b). Comparison shows that the measured growth rates of horizontal scales are larger ($t^{0.40}$ compared to $t^{1/4}$) and that vertical scales are smaller ($t^{0.16}$ compared to $t^{1/2}$) than those of a stable, buoyant lens. The difference arises because bulges are unstable. Stability is evaluated by comparing the ratio, J, of rotational kinetic energy

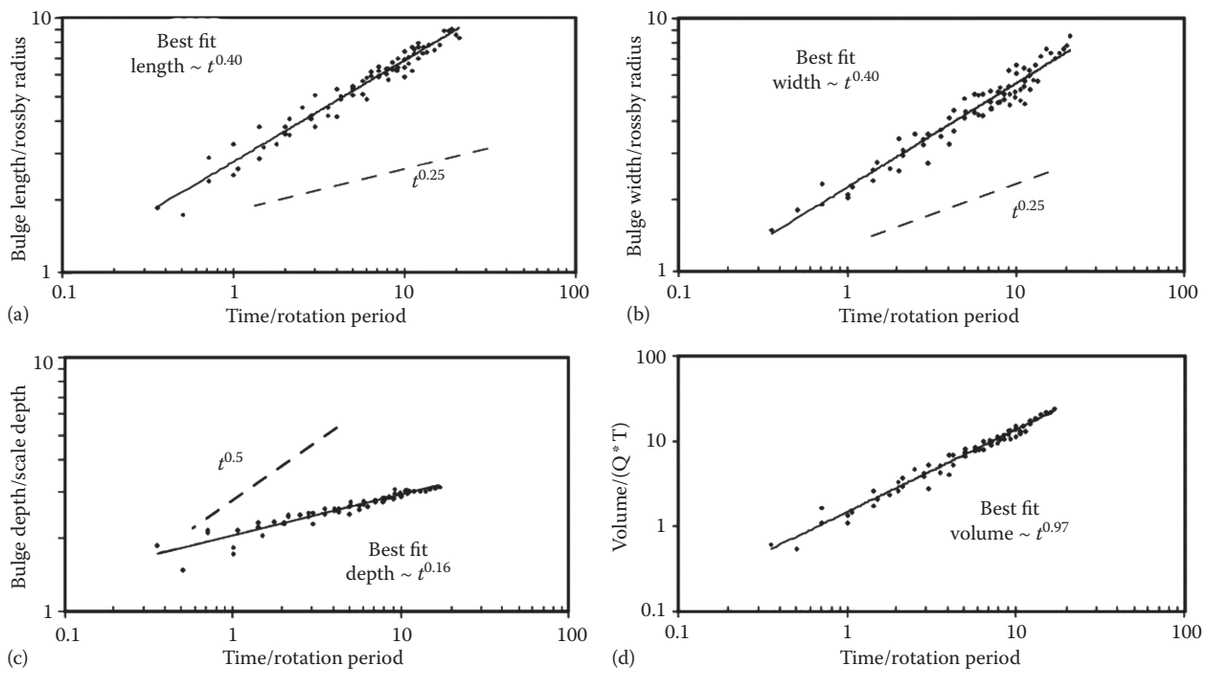

FIGURE 17.9 Evolution of the nondimensional length, width, depth, and volume of bulges. The abscissa is nondimensionalized by the rotation period (numbers correspond to days). In panels (a) and (b) the ordinate is nondimensionalized by the internal Rossby radius R; in panels (c) and (d) the ordinate is nondimensionalized by the scale depth h of the buoyant layer and the product of time t and flow rate Q. Solid lines show the best-fit power laws to the experimental data. Dashed lines are power laws for the evolution of a stable, buoyant lens. The different growth rates for the solid and dashed lines suggest that bulges are unstable. Exit Kelvin number $K_E = W/R = 1$. (Adapted from Avicola, G. and Huq, P., *J. Marine Res.*, 61, 411, 2003b.)

to the available potential energy in the lens ($J = r_b^2 f^2 / g' H_b$, where r_b and H_b are the measured bulge radius and depth at the bulge centerline). Values of the instability parameter J greater than one indicate instability. Measurements indicate that values of $J > 1$ arise as early as time $t < 1T$ (i.e., less than a day, see Figure 17.10 of Avicola and Huq 2003b). Instability augments growth rates in the horizontal direction, but attenuates in the vertical. Observations of the Tsugaru bulge show that it is unstable (Sugimoto 1990).

An important consequence of bulge formation that affects coastal dynamics is the fact that recirculation and growth of the bulge results in storage of outflowing buoyant waters. This storage delays and attenuates the volume of buoyant water propagating downshelf. Without bulge formation, the entire buoyant outflow forms a coastal current that flows downshelf along the coastline. With bulge formation, only about a half of the buoyant outflow is available to form a coastal current. Bulge formation thus impacts the scales of the downshelf propagating coastal current. Data showing this are presented in Figure 17.10. For identical experimental parameters, data are presented for downshelf propagating coastal currents with variations in either the exit angle θ (Figure 17.10a and b) or variations of radius of curvature r_c (Figure 17.10c and d). Comparison show similar evolutions. This provides further support that it is the combined effects of θ and r_c, expressed by the impact angle φ, that is dynamically important. Nondimensional distances (Figure 17.10a and c) propagated by the coastal current for bulge-less outflows are typically 30% larger. Similarly, Figure 17.10b and d show that nondimensional widths of coastal currents for bulge-less outflows are 25% greater than outflows with bulges.

These results can be used to assess aspects of the dynamics of bulges and coastal currents in the ocean. For example, regarding the buoyant outflow at the Tsugaru Strait between Hokkaido and Honshu, Figure 17.2 shows a bulge with circular temperature contours at 200 m with a diameter of about 150 km. Estimates of the internal Rossby radius R and scale depth h for the Tsugaru strait outflow are 16 km and 80 m, respectively, from Table 1 of Avicola and Huq 2002. The data of Figure 17.2 yield a bulge diameter of about 150 km; this corresponds to nondimensional length and width of about 10 R. Figure 17.9a and b indicate that nondimensional length and width of 10 R occur at nondimensional time of 20 days. At 20 days, Figure 17.9c indicates a nondimensional depth of 3 h corresponding to a bulge depth of about 240 m. As local ocean depths are about 300 m, this suggests that the bulge at the Tsugaru Strait is influenced by the proximity of the ocean bottom or may even extend to the ocean bottom.

17.4.3 Scaling of Downshelf Propagating Coastal Currents

The schematics of a downshelf propagating coastal current over a coastal ocean of bottom slope α are presented in Figure 17.11. The depth of the buoyant layer is h, and the depth of the coastal ocean is H. The upper panel shows a relatively thin buoyant layer $h/H < 1$—this configuration is termed surface-advected.

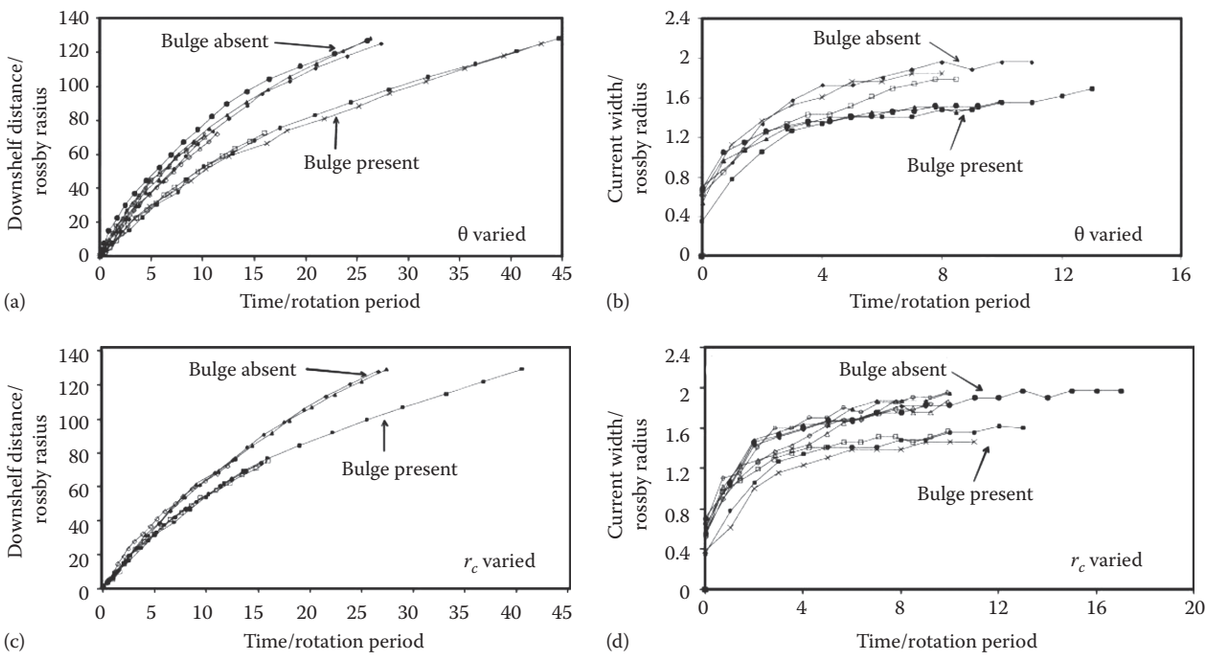

FIGURE 17.10 Evolution of the nondimensional length and width of coastal currents. Ordinate is nondimensionalized by the internal Rossby radius R, and abscissa is nondimensionalized by the rotation period. The exit angle θ was varied in the experiments of panels (a) and (b); the radius of curvature r_c was varied in the experiments of panel (c) and (d). Scales of coastal currents are smaller when bulges are present for all cases due to storage in bulge. Exit Kelvin number $K_E = W/R = 1$. (Adapted from Avicola, G. and Huq, P., *J. Marine Res.*, 61, 411, 2003b.)

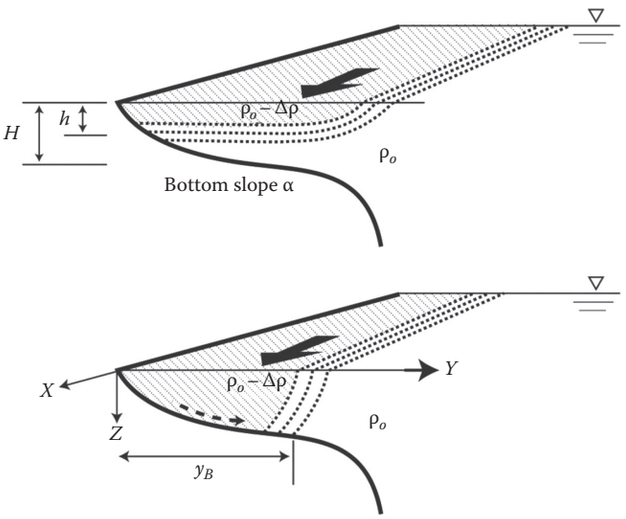

FIGURE 17.11 Schematic of a buoyant coastal current of density ($\rho_o - \Delta\rho$) propagating over a sloping-bottom continental shelf. The scale depth of the buoyant layer is h (see Equation 17.4); the depth of the coastal ocean of density ρ_o is H (defined at an offshore distance approximately equal to the internal Rossby radius R); the slope of the bottom is α. The dashed arrow indicates offshore Ekman transport. The upper panel shows a surface-advected coastal current ($h/H \ll 1$). The lower panel shows a bottom-advected coastal current ($h/H \sim 1$). The dashed arrow denotes offshore Ekman transport; also shown is y_B—the offshore extent at the bottom, or bottom-trapped width, of the buoyant coastal current. (Adapted from Chapman, D.C. and Lentz, S.J., *J. Phys. Oceanog.*, 24, 1464, 1994.)

The lower panel shows the case where the buoyant layer extends to the bottom so that $h/H = 1$—a bottom-advected case. The dashed arrow at the bottom of the lower panel indicates offshore transport of buoyant water by a thin Ekman layer. The buoyant layer above the Ekman layer is in geostrophic balance. The Ekman layer extends to a distance y_B offshore—the location at which the downshelf velocity of the geostrophic layer vanishes at the level of the Ekman layer.

The flow configuration of Figure 17.11 was analyzed by Lentz and Helfrich (2002) and Avicola and Huq (2002). They recognized the important role of the bottom Ekman layer as an additional flow pathway that transports buoyant water in the offshore direction. The dynamics of the flow were characterized by a two-variable nondimensional parameter space: the ambient depth parameter, h/H, and the bottom-slope parameter R/y_B. The ratio h/H is the fraction of the available depth H occupied by the buoyant layer. The scale depth, h, derived from geostrophic dynamics, is a measure of the depth of the buoyant layer. The bottom-slope parameter is the ratio of two horizontal scales, the internal Rossby radius, R, to the bottom-trapped width y_B. An estimate for y_B is

$$y_B \sim \frac{f\rho}{\alpha g}\frac{u_{\max}}{\partial\rho/\partial y} \tag{17.5}$$

here $u_{\max}$ is the downshelf propagation speed of the leading edge or nose of the coastal current (see Figure 17.3). Scaling by Equation 17.4 reduces Equation 17.5 to the simple form $y_B \sim h/\alpha$. Thus in nondimensional form, the bottom-slope parameter is

$$\frac{R}{y_B} = \frac{\alpha R}{h} \tag{17.6}$$

Noting that the average isopycnal slope in the buoyant layer is h/R, we find that the bottom-slope parameter R/y_B can also be interpreted as the ratio between the bottom slope α and the average isopycnal slope h/R. (See Avicola and Huq [2002] for discussion and derivation of Equation 17.5.)

The two parameter space (h/H, R/y_B) together with observations of coastal currents values of the parameters are plotted on Figure 17.12. For an idealized coastal ocean with a single bottom slope α, R/y_B and h/H are related through the definition of H ($= \alpha R$). The only possible values in the parameter space falls on the line $h/H = (R/y_B)^{-1}$, which is shown as a dashed line on Figure 17.12. Values of coastal current parameters are constrained to lie below the line $h/H = (R/y_B)^{-1}$ for realistic coastal bottom bathymetry. Increasing values of the depth parameter h/H reflects increasing interaction between the coastal current and the bottom bathymetry. Coastal currents with $h/H \sim 0.1$ are isolated from the bottom (surface-advected); on the other hand, coastal currents with $h/H \sim 1$ are bottom-trapped with pronounced offshore transport of buoyant waters via the bottom Ekman layer.

A consequence of offshore transport of buoyant water is attenuation of downshelf propagation speed of coastal currents. Thus in the limit of bottom-trapped coastal currents, propagation speed $u_{\max}$ is set (slope-controlled) by the slope as ($\alpha g'/f$). Isopycnal slopes are flattened and isopycnal gradients $\partial\rho/\partial y$ are weakened if y_B is smaller than R. That is coastal currents undergo lateral expansion for $R/y_B < 1$. For $R/y_B > 1$ coastal currents are compressed closer to the shore.

The framework of the two parameter space (h/H, R/y_B) for the scaling of coastal currents has been tested and verified via both

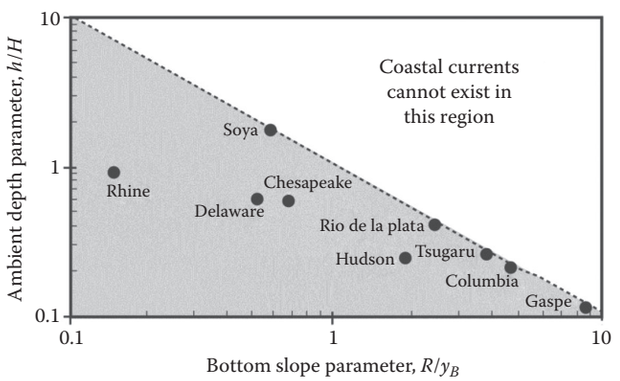

FIGURE 17.12 Log–log plot of field data of coastal currents plotted in the parameter space (h/H, R/y_B). Field data lie below the line $h/H = (R/y_B)^{-1}$ in agreement with scaling arguments. (Adapted from Avicola, G. and Huq, P., *J. Phys. Oceanog.*, 32(11), 3233, 2002.)

laboratory experiments and coastal ocean data. First, characteristics of surface-advected coastal currents ($h/H \sim 0.1$) are independent of the value of the bottom-slope parameter R/y_B. In contrast, the evolution of downshelf propagation distance and offshore extent varied with whether the value of R/y_B was greater or less than one for bottom-trapped coastal currents ($h/H \sim 1$). And second that coastal current propagation speeds varied with the slope as ($\alpha g'/f$). Available data of coastal currents fall in the permissible half-space below the line $h/H = (R/y_B)^{-1}$ on Figure 17.12. Finally, density transects through both laboratory and oceanic coastal currents confirm that isopycnal slopes are of order (R/h).

17.5 Major Challenges

The fluid dynamics of buoyant outflows to the coastal ocean is a complex interplay between buoyancy, rotation, friction, pressure gradients, and coastline geometry. The approach of analysis of the transport of momentum and buoyancy based on steady, depth-averaged hydrodynamic equations combined with scaling analysis and exploration of the parameter space via laboratory experiments has yielded insights and useful results. However, a weakness of such approaches, as noted by Garvine (1995), is that it relies on the knowledge of coastal current scales such as the depth of the buoyant layer, h, the internal Rossby radius, R, and internal wave phase speed, c. A goal for the future is to develop approaches for predicting the characteristics of coastal currents based on the knowledge of far upstream hydrography. Some outstanding issues that seem within reach are discussed in the following to conclude this review.

An obvious shortcoming of the approach taken here is the assumption of a steady flow. Oceanographic observations of buoyant outflows show that flow rates vary seasonally through the year. Thus a time-averaged approach is an oversimplification. The bulge can also be unstable. More work on the mechanics of the instability is needed as instability influences transport and mixing between buoyant outflow and ambient coastal waters. Tidal time scales are also likely to be important. While it is known that tides stabilize bulge formation, the effect of tides on other aspects of the outflow is unknown.

Meteorological variability and its impact on the dynamics of bulges and coastal currents is another unresolved issue. The trajectory of the Columbia River buoyant outflow varies with seasonal wind direction—it flows to the north in the winter and to the south in the summer. Thus the effects of the variability of wind direction (and strength) need to be assessed. The structure of the buoyant outflows from Delaware Bay and Hudson River can be disrupted by upshelf (upwelling) winds, with the result that buoyant waters can move upshelf and offshore. Conversely, propagation speeds of coastal currents are augmented by winds blowing downshelf.

The depth of the wind-driven surface Ekman layer may differ from the depth of the buoyant layer. Thus it is likely that the effect of winds on very large-scale buoyant outflows such as the Tsugaru (flow rates $Q \sim 10^6\,m^3/s$) will differ from smaller-scale outflows such as the Rhine, Chesapeake, and Delaware outflows where $Q \sim 10^3\,m^3/s$. The effects of persistence or duration of winds is also unknown. A third issue of meteorological variability on the dynamics of buoyant outflows is the question of baroclinic forcing due to inputs of buoyancy at the sea surface. This has not been addressed; however, it is likely to alter the potential energy anomaly due to the density contrast between the buoyant waters and the ambient coastal ocean. Clearly, meteorological variability is a critical issue.

Another question that needs to be addressed is the interaction between buoyant outflows and the larger-scale coastal circulation. For example, how do ambient shelf currents impact bulge formation and propagation of buoyant coastal currents? The focus of recent work has concerned outflows equal in exit width, W, to the internal Rossby radius (i.e., $K_E = W/R = 1$). Typically, in these studies the velocity profile of the buoyant outflow is laterally uniform. Recent numerical and laboratory experiments of wide outflows $K_E > 1$ by Valle-Levinson (2008) and Huq (2009) show that lateral velocity shear can arise if frictional effects are significant. They also found that rotation produces separation of the buoyant outflow from the left-hand side (looking seaward) of the outflow. This results in dynamical isolation of the outflow and inflow—buoyant outflow occurs on the right-hand side (looking seaward) and inflow on the left. (Reverse left and right in the southern hemisphere.) Surprisingly, little attention has been paid to the dynamics associated with inflow. Inflow and attendant mixing will alter the density field upstream of the outflow exit. The density of the buoyant outflow will obviously depend on the inflow and mixing within the estuary. Wide estuaries have room for expansion: thus differential advection, tidal straining, and secondary circulation may play even more surprising roles than they do for a $K_E = 1$ buoyant outflow. To reiterate, flow pathways for wide estuaries ($K_E > 1$) differ from that of narrow estuaries ($K_E \sim 1$). It will be useful to determine the characteristics of and magnitude of transport through these flow pathways, and their dependence upon width and friction, parameterized by K_E and h/H.

The picture emerging from this review of buoyant outflows to the coastal ocean is of deterministic coherent structures such as bulges and coastal currents constituting flow pathways in the coastal ocean. Such flow pathways determine the transport and dispersion of pollution, and distribution and deposition of embedded sediments on the continental shelf. As they impact the biology and productivity of coastal waters, bulges and coastal currents are vital components of the health of the fragile coastal environment.

References

Avicola, G. and P. Huq, 2002, Scaling analysis for the interaction between a buoyant coastal current and the continental shelf: Experiments and observations, *Journal of Physical Oceanography*, 32(11), 3233–3248.

Avicola, G. and P. Huq, 2003a, The characteristics of the recirculating bulge region in coastal buoyant outflows, *Journal of Marine Research*, 61, 435–463.

Avicola, G. and P. Huq, 2003b, The role of outflow geometry in the formation of the recirculating bulge region in coastal buoyant outflows, *Journal of Marine Research*, 61, 411–434.

Brink, K.H. and A.R. Robinson, eds., 1998, *The Sea Volume 10: The Global Coastal Ocean*, John Wiley & Sons, New York, p. 604.

Chapman, D.C. and S.J. Lentz, 1994, Trapping of a coastal density front by the bottom boundary layer, *Journal of Physical Oceanography*, 24, 1464–1479.

Garvine, R.W., 1995, A dynamical system for classifying buoyant coastal discharges, *Continental Shelf Research,* 15, 1585–1596.

Horner-Devine, A., D.A. Fong, S.G. Monismith, and T. Maxworthy, 2006, Laboratory experiments simulating a coastal river inflow, *Journal of Fluid Mechanics*, 555, 203–232.

Huq, P., 2009, The role of Kelvin number on bulge formation from estuarine buoyant outflows, *Estuaries and Coasts,* 32, 709–719.

Kawasaki, Y. and T. Sugimoto, 1984, Experimental studies on the formation and degeneration process of the Tsugaru Warm Gyre, in *Ocean Hydrodynamics of the Japan and East China Seas*, ed. T. Ichiye. Oceanography Series. No. 39, Elsevier, Amsterdam, the Netherlands, pp. 225–238.

Lentz, S.J. and K.R. Helfrich, 2002, Buoyant gravity currents along a sloping bottom in a rotating fluid, *Journal of Fluid Mechanics*, 464, 251–278.

Nof, D. and T. Pichevin, 2001, The ballooning of outflows, *Journal of Physical Oceanography*, 31, 3045–3058.

Sugimoto, T., 1990, A review of recent physical investigation of straits around the Japanese Islands, in *The Physical Oceanography of Sea Straits*, ed. L.J. Pratt, Kluwer Academic, Dordrecht, the Netherlands.

Valle-Levinson, A., 2008, Density-driven exchange flow in terms of the Kelvin and Ekman numbers, *Journal of Geophysical Research*, 113(C5), doi:1029/2008JC004853.

Whitehead, J.A., 1985, The deflection of a baroclinic jet by a wall in a rotating fluid, *Journal of Fluid Mechanics*, 157, 79–93.

Yankovsky, A.E. and D.C. Chapman, 1997, A simple theory for the fate of buoyant coastal discharges, *Journal of Physical Oceanography*, 27, 1386–1401.